AIP Journal of Applied Physics

Electrical and optical properties of beryllium-implanted Mg-doped GaN

Chang-Chin Yu, C. F. Chu, J. Y. Tsai, C. F. Lin, and S. C. Wang

Citation: Journal of Applied Physics **92**, 1881 (2002); doi: 10.1063/1.1494110
View online: http://dx.doi.org/10.1063/1.1494110
View Table of Contents: http://scitation.aip.org/content/aip/journal/jap/92/4?ver=pdfcov
Published by the AIP Publishing

Articles you may be interested in

Low resistance, unannealed, Ohmic contacts to p -type In 0.27 Ga 0.73 Sb a)
J. Vac. Sci. Technol. B **24**, 2388 (2006); 10.1116/1.2353838

Investigation of degradation for ohmic performance of oxidized Au/Ni/Mg-doped GaN
Appl. Phys. Lett. **82**, 2817 (2003); 10.1063/1.1569991

Influence of microstructure on the carrier concentration of Mg-doped GaN films
Appl. Phys. Lett. **79**, 2734 (2001); 10.1063/1.1413222

Reactivation of Mg acceptor in Mg-doped GaN by nitrogen plasma treatment
Appl. Phys. Lett. **76**, 3079 (2000); 10.1063/1.126585

Structural defects and microstrain in GaN induced by Mg ion implantation
J. Appl. Phys. **83**, 5992 (1998); 10.1063/1.367465

Re-register for Table of Content Alerts

Create a profile.

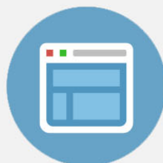

Sign up today!

[This article is copyrighted as indicated in the article. Reuse of AIP content is subject to the terms at: http://scitation.aip.org/termsconditions. Downloaded to] IP: 140.113.38.11 On: Thu, 01 May 2014 06:11:38

JOURNAL OF APPLIED PHYSICS VOLUME 92, NUMBER 4 15 AUGUST 2002

Electrical and optical properties of beryllium-implanted Mg-doped GaN

Chang-Chin Yu, C. F. Chu, J. Y. Tsai, C. F. Lin, and S. C. Wang[a)]
Institute of Electro-Optical Engineering, National Chiao Tung University, Hsinchu, Taiwan, Republic of China

(Received 2 January 2002; accepted for publication 24 May 2002)

We investigated the electrical and optical characteristics of beryllium implanted Mg-doped GaN materials. The Mg-doped GaN samples were grown by metalorganic chemical vapor deposition system and implanted with Be ions at two different energies of 50 and 150 keV and two different doses of about 10^{13} and 10^{14} cm^{-2}. The implanted samples were subsequently rapidly thermal annealed at 900, 1000, and 1100 °C for various periods. The annealed samples showed an increase of hole concentration by three orders of magnitude from nonimplanted value of 5.5×10^{16} to 8.1×10^{19} cm^{-3} as obtained by Hall measurement. The high hole concentration samples also showed low specific resistance ohmic contact of about 10^{-3} $\Omega\,cm^2$ and 10^{-6} $\Omega\,cm^2$ using Ni/Au and Ni/Pd/Au metallization, respectively, without any further annealing process. It is also found from the temperature dependent photoluminescence that the activation energy of Mg dopants of the Be implanted samples has an estimated value of about 170 meV, which is nearly 30% lower than the as-grown samples of about 250 meV. The crystal quality and surface morphology of the Be implanted samples measured by x-ray diffraction and atomic force microscopy show no obvious degradation in the crystal quality and surface morphology. © *2002 American Institute of Physics.*
[DOI: 10.1063/1.1494110]

I. INTRODUCTION

The group III nitride semiconductors,[1,2] especially Gallium nitride (GaN), have been successfully employed to realize blue-green light-emitting diodes and blue laser diodes,[3–7] UV light sources and detectors.[8–11] In order to fabricate these devices, it is necessary to implement controllable doping of GaN to realize both *n*-type and *p*-type GaN. Generally, *n*-type GaN has been achieved with the doping of Si[12] and *p*-type GaN is typically achieved by doping magnesium in metalorganic chemical vapor deposition (MOCVD) or molecular beam epitaxy. However, the performance of such light-emitting diodes and lasers remains limited by several problems related to the formation of low-resistance ohmic contact to the *p*-type GaN. The primary reasons are the relative high optical activation energy of Mg of around 250 meV[1] and the formation of Mg–H complexes[13–15] during MOCVD growth. These have usually been suggested to be responsible for the low activation efficiency of Mg that results in the relative low *p*-type GaN carrier concentration and high *p*-contact resistance compared to that of *n*-type GaN. Most of the reported methods for reducing *p* contact resistance rely on the improvement of metal-semiconductor interface[16–18] and optimization of the contact annealing temperature. The activation of Mg acceptors is generally very low and limited to activation ratio of about 10^{-2}–10^{-3} for Mg doping levels between 10^{18} and 10^{21} cm^{-3}. Therefore, a high activation efficiency *p*-dopant is desirable. Beryllium has low theoretical activation energy of about 60 meV[19] making it a promising candidate for *p*-type doping in GaN. We adopt the ion implantation procedure for doping Be into GaN, because it can provide precise control of dopant concentration and depth distribution. It is also easier to incorporate Be into GaN than the MOCVD process. A number of studies on the ion implantation of undoped GaN have been reported earlier, including the thermal stability,[20,21] electrical activation[22] of the implanted species, and the radiation damages[23] were investigated as a function of annealing temperature and condition. The implantation of Be ions in GaN materials showed the implanted ions did not diffuse for the annealing temperature up to 800 °C.[21–21] Photoluminescence (PL) spectra of Be implanted GaN were earlier reported by Pankove and Hutchby[24] and observed the Be-related peak at 520 nm. However, so far there are no mentions on the implantation of *p*-doped GaN. In this article, we discuss the results of Be implantation in Mg-doped GaN including the optical, electrical properties and surface morphology, and achievement of high carrier concentration, low specific resistance, and reduction in Mg dopant activation energy.

II. EXPERIMENT

The Mg-doped GaN samples were grown on *c*-axis sapphire substrates by MOCVD at 1080 °C. Prior to 1-μm-thick Mg-doped GaN layer growth, a 1.0–3.0 μm high temperature undoped GaN and 30-nm-thick low temperature GaN buffer layer was first deposited on the substrate. Trimethylgallium, ammonia, and CP_2Mg were used as Ga, N, and Mg sources, respectively. These samples were separated into two sets. Firsts set was post-growth annealed for 40 min at 700 °C, while the second was not post-growth annealed. The initial hole concentration and mobility at room temperature for post-growth annealed samples before Be implantation were made by Hall measurements to be 5.5×10^{16} cm^{-3} and

[a)]Author to whom correspondence should be addressed; electronic mail: scwang@cc.nctu.edu.tw

 © 2002 American Institute of Physics

[This article is copyrighted as indicated in the article. Reuse of AIP content is subject to the terms at: http://scitation.aip.org/termsconditions. Downloaded to] IP: 140.113.38.11 On: Thu, 01 May 2014 06:11:38

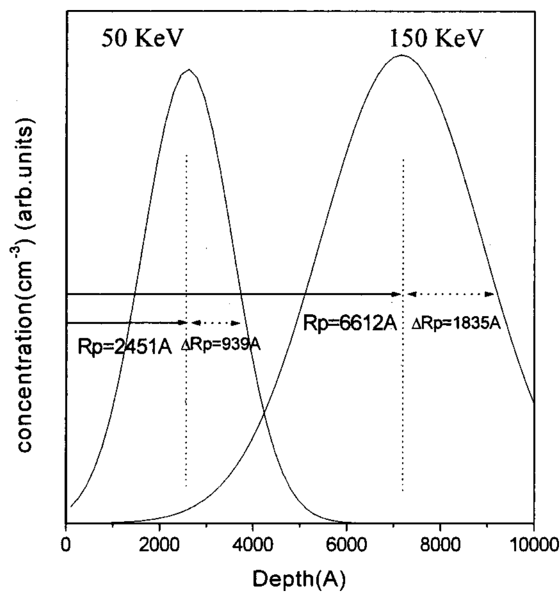

FIG. 1. TRIM stimulation of the ion projection ranges (Rp) and the straggles (ΔRp) for Be ions implanted into 1 μm p-type GaN with implantation energy of 50 and 150 keV.

7.6 $cm^2 v^{-1} s^{-1}$, respectively. These two sets of samples were subsequently implanted with Be ions at two different energies of 50 and 150 keV and two different doses of about 10^{13}, 10^{14} cm^{-2}. The ion projection ranges for energy 50 and 150 keV were estimated to be about 0.25 and 0.66 μm, respectively, while the straggles were about 0.09 and 0.18 μm, respectively by the TRIM simulation[25] as shown in Fig. 1. These implanted samples were subsequently rapidly thermal annealed (RTA) at 900, 1000, and 1100 °C for various periods in N_2 ambient. Since a recent report[26] indicated the loss of nitrogen when the GaN sample was annealed above 1000 °C without surface protection. Our samples were capped with undoped GaN during the RTA process to prevent the samples dissociation.

The carrier concentration of these samples was determined by Hall measurement at room temperature. The as-grown samples with dimension of 7×7 mm^2 were cut from the wafer first and metal (Ni/Au) dots were then evaporated in the four corner to obtain electrical contacts in the Van der Pauw geometry. The metal contact was rapidly thermal annealed at 500 °C, 30 s in the ambient gas of N_2 to obtain ohmic contact for Hall measurement. The PL measurements were obtained at temperatures ranging from 20 to 300 K using a 325 nm He-Cd laser excitation source. The x-ray diffraction experiments were performed using a high-resolution x-ray diffractometer with the Cu K_β ($\lambda=1.541$ A) line. The surface morphology of all samples was examined by an atomic force microscopy (AFM).

From the AFM data, the surface roughness of the as-grown samples and two sets of samples with different RTA temperatures have rms values ranging from 0.5 to 2.5 nm. This value is comparable with the surface roughness of typical the Mg-doped GaN sample grown by MOCVD.[27] This result suggests that the implantation and RTA process seem to cause no major degradation in the sample surface morphology. The use of an undoped GaN as a cap during RTA process in our experiment could have effectively prevented the surface dissociation of GaN and maintained the good surface morphology after the process.

III. RESULTS AND DISCUSSION

A. Photoluminescence and x-ray diffraction spectra

The PL spectra of the as-grown and as-implanted samples were shown in Fig. 2(a). The spectra have several typical Mg-related emission lines at 380 nm (3.26 eV), 392 nm (3.16 eV), 402 nm (3.08 eV), 420 nm, (2.95 eV), 440 nm (2.8 eV), and 465 nm (2.67 eV) similar to those reported earlier.[28,29] The 380 nm (3.26 eV) peak was assigned to the donor–acceptor pair (DAP) zero-phonon emission of Mg and the 392 nm (3.16 eV), and 402 nm (3.08 eV) peaks were those of the DAP phonon replicas with an energy separation of about 90 meV. The DAP line is attributed to native donor-to-shallow Mg-related acceptor transition and the involved acceptor level is of about 200–250 meV deep from the valence band.[1,30,31] A broad blue band at 420 nm (2.95 eV), 440 nm (2.8 eV) was also attributed to DAP-type transitions from the deeper donors to the identical shallow acceptor. Additionally, a deeper Mg-related acceptor level of about 530 meV from the valence band corresponding to 465 nm (2.67 eV) transitions is considered to be due to randomly dispersed deep acceptors, defects, and impurities such as V_{Ga}, V_N, Mg_{Ga}, O_N, and Mg complexes.[32,33] As shown in Fig. 2(a), the intensity of these PL lines becomes much weaker after the implantation, indicating the occurrence of possible lattice damages due to the implantation.

These implanted samples were subsequently rapidly thermal annealed at 900, 1000, and 1100 °C for various periods of 15, 30, 45, and 60 s, to repair the implantation-induced damages and to establish optimum annealing conditions. Figure 2(b) shows the PL spectra of the first set of samples for the various annealing periods at 1100 °C. The PL spectra shows an additional broad spectrum near 520 nm that is different from traditional yellow band, and is considered to be related to the lattice disorders induced by ion implantation,[34] such as V_{Ga}, V_N, and Be complexes. As the annealing period increases, the implantation damage related 520 nm peak is gradually quenched and the 420 and 440 nm peaks are also enhanced. This suggests that the implantation-induced damages are repaired by the RTA process. To further quantify the effect of annealing on the samples, we set the intensity ratio of 420 nm line and the broad band at 520 nm, $I_{420\ nm}/I_{520\ nm}$ as a measure of the relative repair condition of the implantation induced damages. Figure 3 shows the variation of the intensity ratio $I_{420\ nm}/I_{520\ nm}$ as a function of annealing conditions for the first set samples. As can be seen, the intensity ratio has no apparent change for annealing temperature at 900 and 1000 °C. However, at annealing temperature of 1100 °C, the intensity ratio changes rapidly with annealing time up to 60 s. This result clearly indicates that the implantation-induced damages could be repaired by RTA at 1100 °C. Therefore, all the second set implanted samples were annealed at 1100 °C for 60 s.

The x-ray rocking curve (XRC) spectra shown in Fig. 4 show the effect of annealing temperature and periods on the

[This article is copyrighted as indicated in the article. Reuse of AIP content is subject to the terms at: http://scitation.aip.org/termsconditions. Downloaded to] IP: 140.113.38.11 On: Thu, 01 May 2014 06:11:38

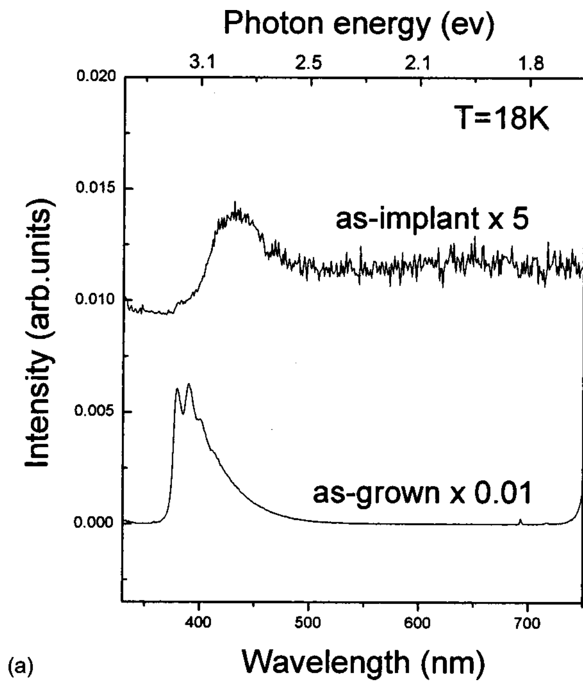

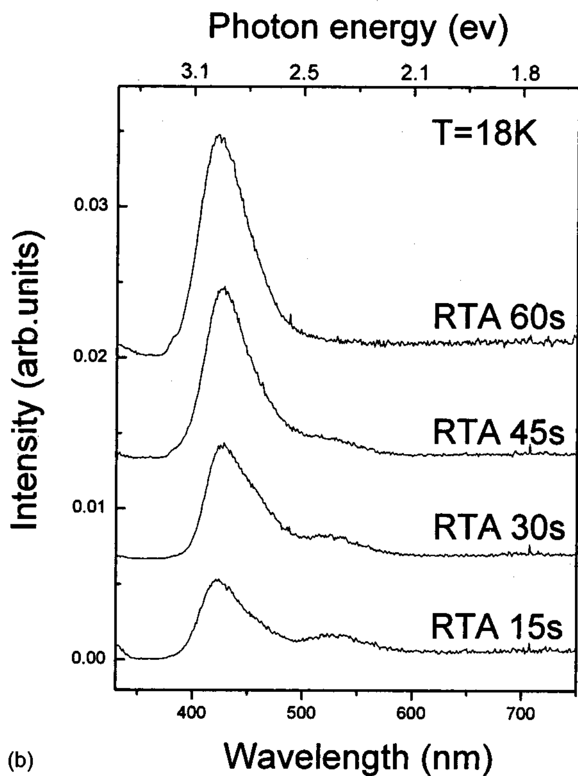

FIG. 2. (a) PL spectra of the as-grown and as-implanted samples, and (b) PL spectra of the Be implanted p-type GaN samples with annealing temperature of 1100 °C for various annealing periods.

implanted samples. It can be seen that the full width half maximum (FWHM) decreases as the annealing temperature is raised to 1100 °C and becomes lower than the as-grown sample. This data further substantiates the repair of the implantation induced damages during RTA process at 1100 °C and the possible filling of Be ions into the native vacancies and repair of the vacancy defects.

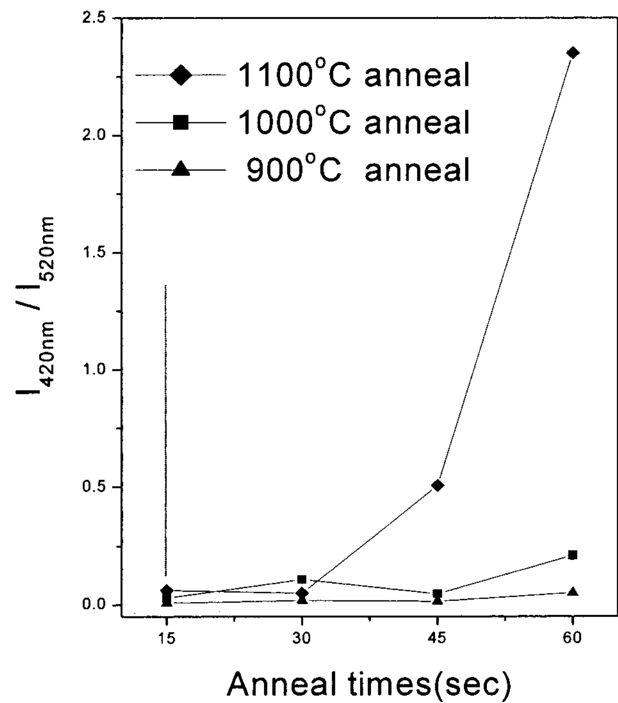

FIG. 3. The intensity ratio $I_{420\ \mathrm{nm}}/I_{520\ \mathrm{nm}}$ vs annealing time for Be implanted samples at implantation energy of 50 keV.

B. Temperature dependent of PL spectrum

To examine the effect of Be implantation on Mg-doped GaN samples, we measured the temperature dependence of the PL spectra for the first set of samples before Be ions implantation as shown in Fig. 5(a). The 380 nm peaks with phonon replica is barely resolved below 50 K and the broad band at 420 and 440 nm are dominated in the PL spectra. We plotted in Fig. 5(b) the relation between the logarithms of the

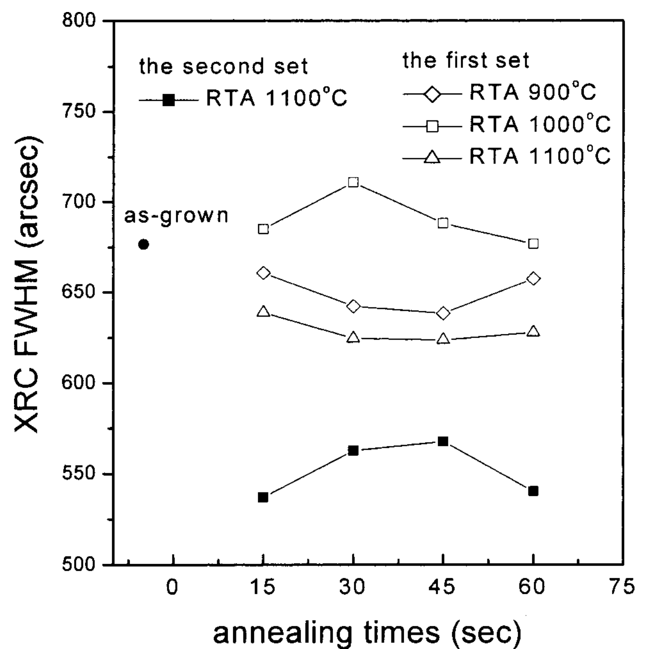

FIG. 4. The FWHM of XRC for the as-grown, the first and second set samples with different annealing temperature for various annealing periods.

[This article is copyrighted as indicated in the article. Reuse of AIP content is subject to the terms at: http://scitation.aip.org/termsconditions. Downloaded to] IP: 140.113.38.11 On: Thu, 01 May 2014 06:11:38

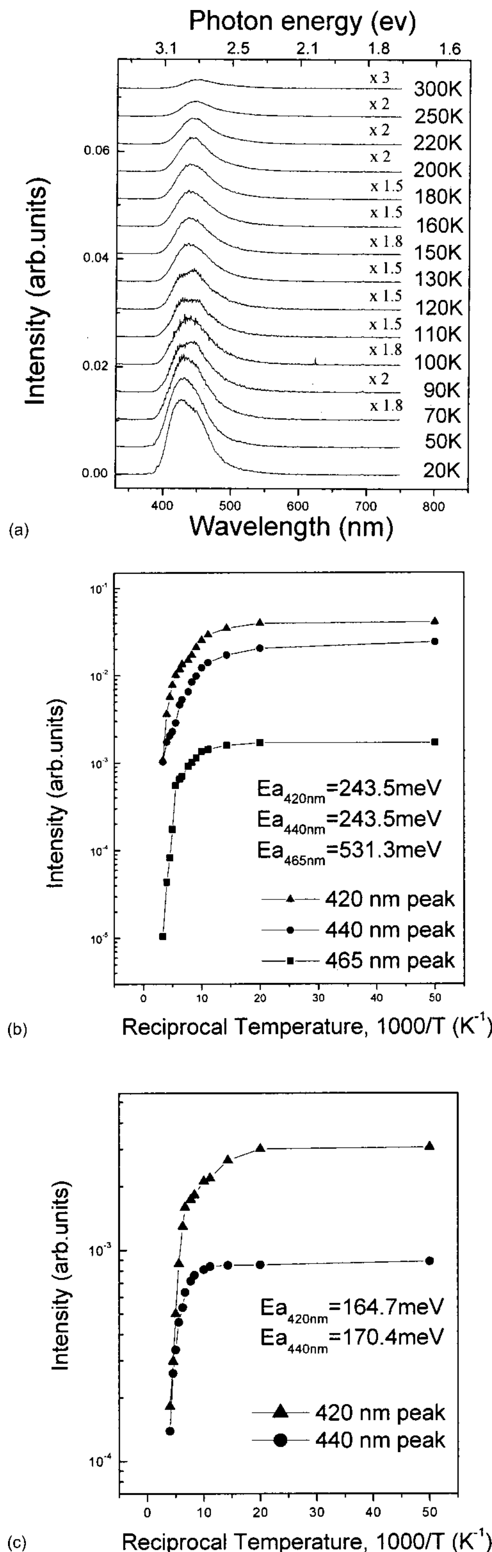

FIG. 5. (a) PL spectra of the Mg-doped GaN samples with post-growth annealing (the first set) before Be ions implanted at various temperatures. (b) Temperature dependent of PL intensity for the first set samples before Be ions implantation at 420, 440, and 465 nm emission lines, and the Arrhenius plot of the data. (c) Temperature dependent of PL intensity for annealed implanted samples (the second set) at 420 and 440 nm emission lines, and the Arrhenius plot of the data.

DAP emission of Mg at 420, 440, and 465 nm bands and the reciprocal temperatures. We also measured the temperature dependence of the PL spectra for the second set samples after Be ion implantation with the same RTA condition at 1100 °C for 60 s. The relation between the logarithms of the DAP emission of Mg and reciprocal temperature is shown in Fig. 5(c). Both Fig. 5(b) and Fig. 5(c) show that the PL emission intensity at these wavelengths is nearly constant below the temperature 100 K. The emission intensity then decreases rapidly with the increasing temperature above the temperature 100 K. The variation of the emission intensity I with temperature T shown in Fig. 5(b) and Fig. 5(c) for both sets of samples can be fitted by the Arrhenius function[35] of form

$$I(T)=\frac{I(0)}{1+C_1\exp(-E_{a1}/kT)+C_2\exp(-E_{a2}/kT)},$$

where C_1, C_2 are constants, E_{a1} is the activation energy of Mg dopants, and E_{a2} is generally assigned as free exciton binding energy. For the first set samples, we obtained an estimated activation energies of about 243.5 meV for 420 and 440 nm bands, while the 465 nm peak has an activation energy of about 531.3 meV.[36] These results agreed with earlier reported[37] that p-type GaN with Mg doping has one shallow and another deeper Mg-related acceptor level. However, from the curve fitting of the second set samples, we obtain an activation energy of about 170 meV, which his about 30% lower than that of the first set samples. This result suggests that the implantation of Be has an effect of reduction of Mg activation energy, which can result in increasing the dopant activation efficiency.

C. Carrier concentration and specific resistance

Figure 6(a) shows the carrier concentration of the first set Be implanted samples with post-growth annealing at implantation energy of 50 keV and dose of 10^{14} cm^{-2} at different annealing temperatures of 900, 1000, 1100 °C and for annealing periods of 15, 30, 45, and 60 s. The result clearly showed no apparent change of the carrier concentration for annealing temperatures of 900 and 1000 °C. However, at the annealing temperature of 1100 °C, the carrier concentration increases rapidly with annealing time up to 60 s and reaches value of about 2.3×10^{19} cm^{-3}. This result is consistent with the Fig. 3 PL measurements for the first set samples.

Figure 6(b) shows the variations of the carrier concentration with annealing periods for the second set Be implanted samples for different implantation energies and dosages at annealing temperature of 1100 °C. The carrier concentration increases with annealing periods for all samples. The samples with implantation energy of 50 keV have higher hole concentration than that of 150 keV. For the 50 keV implanted samples, the carrier concentration reached a highest value of about 8.1×10^{19} cm^{-3} for a dose of 10^{14} cm^{-2},[38] while with a dose of 10^{13} cm^{-2} the carrier concentration is about 1.8×10^{19} cm^{-3}. As for the 150 keV implanted samples, the highest carrier concentration for dose of 10^{13} cm^{-2} is about 3.1×10^{19} cm^{-3}. This result suggests that low implantation energy with a higher dose is better for achieving high hole concentration. The hole mobility of these two sets of samples was also measured to be in the range of $1\sim3$ cm^2 V^{-1} s^{-1}, with no particular dependence on annealing temperature.

[This article is copyrighted as indicated in the article. Reuse of AIP content is subject to the terms at: http://scitation.aip.org/termsconditions. Downloaded to] IP: 140.113.38.11 On: Thu, 01 May 2014 06:11:38

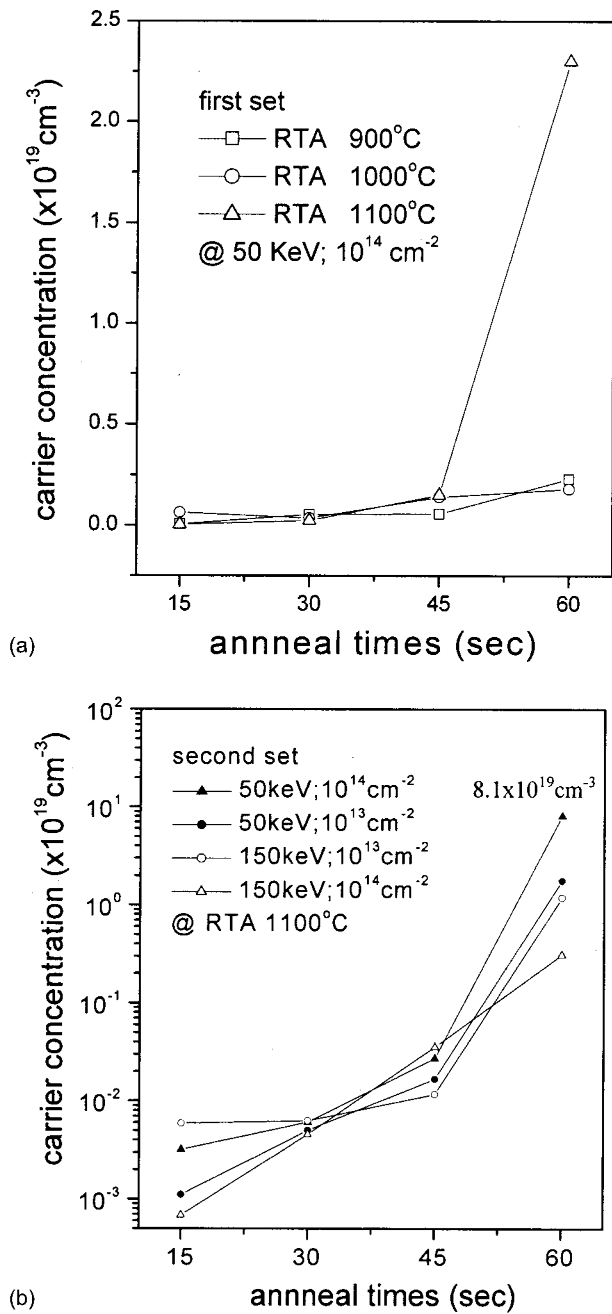

FIG. 6. (a) Carrier concentration versus annealing time for Be implanted samples with post-annealing (the first set) for different annealing temperature and various periods, and (b) carrier concentration versus annealing time for Be implanted samples without post-annealing (the second set) for different implantation energy and dosage at annealing temperature of 1100 °C.

For comparison, we performed the experiment using the as-grown Mg–GaN samples. These samples were annealed at 900, 1000, 1100 °C for annealing periods of 15, 30, 45, and 60 s. The results show no major increase in the carrier concentration and mobility with typical values of about $1\times 10^{17}\ \mathrm{cm}^{-3}$ and $5\ \mathrm{cm}^2\,\mathrm{v}^{-1}\,\mathrm{s}^{-1}$, respectively. Additionally, we also performed the experiment on implantation of Be on unintentionally doped GaN under the same annealing conditions at 900, 1000, and 1100 °C for various periods. All the samples showed *n*-type property similar to the results reported by S. J. Pearton *et al.*[3] earlier. This result was believed to be caused by the implantation induced defects which have the donor property and compensate the Be acceptors. These experiments confirm the implantation of Be is the major cause of the dramatic improvement in carrier density of the Mg–GaN samples. The exact mechanism of high hole concentration is not fully understood yet. However, there are two possible mechanisms that could be responsible for high hole concentration. According to Ref. 27, the Be ion can capture H much more easily than Mg facilitating the activation of Mg. Furthermore, from the temperature dependent PL data, the Mg activation energy was reduced after Be implantation. This could allow Mg to release the hole more efficiently and increase the activation ratio.

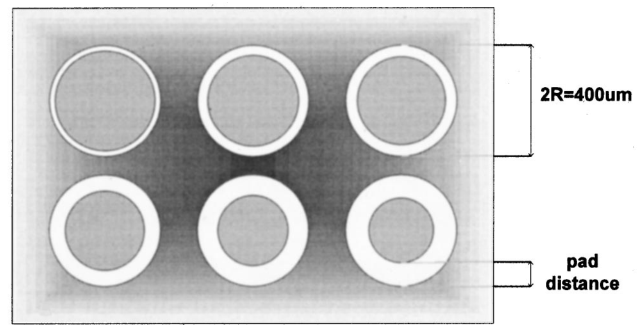

FIG. 7. Circular transmission line method (CTLM) pattern with the inner dot radius of 200 μm, and the spacing between the inner and the outer radii were varied from 3 to 45 μm.

The specific contact resistance of these samples was investigated using circular transmission line method (CTLM). The CTLM pattern is shown in Fig. 7. Both circular and annular pads were patterned on the samples by the standard photolithography technique for measurement of specific contact resistance. The inner dot radius was 200 μm and the spacing between the inner and the outer radii were varied from 3 to 45 μm. Two types of metal contact layer structure using a new metallization of Ni (20 nm)/Pd (20 nm)/Au (100 nm),[39] and a typical metallization of Ni (20 nm)/Au (100 nm) were deposited on both sets of *p*-type GaN samples with high hole carrier concentration of $8.1\times 10^{19}\ \mathrm{cm}^{-3}$ and $2.3\times 10^{18}\ \mathrm{cm}^{-3}$ by electron beam evaporation under a pressure of 2×10^{-6} Torr. Without any further annealing process after the contact metallization, both samples illustrate near perfect linear $I-V$ characteristics as depicted in Fig. 8(a). Total resistance (Y) measured by CTLM has a linear relation with pad distances (X) as shown in Fig. 8(b). The specific contact resistance ρ_c was determined from following the linear relationship equation, $Y=2R_c+\rho_s/2\pi R\times X$ and the relation between the specific resistance and the sheet resistance $\rho_c=\rho_s\times L_T^2$, where R_c is the contact resistance, ρ_s is the sheet resistance, and L_T is the transfer length. By fitting the data we obtain a very low specific contact resistance value of $4.5\times 10^{-6}\ \Omega\,\mathrm{cm}^2$ for the sample with a carrier concentration of $8.1\times 10^{19}\ \mathrm{cm}^{-3}$ using Ni/Pd/Au metallization, while for the sample with a carrier concentration of $2.3\times 10^{18}\ \mathrm{cm}^{-3}$ using the typical Ni/Au metallization, it can also reach a low specific contact resistance value of 6.9

[This article is copyrighted as indicated in the article. Reuse of AIP content is subject to the terms at: http://scitation.aip.org/termsconditions. Downloaded to] IP: 140.113.38.11 On: Thu, 01 May 2014 06:11:38

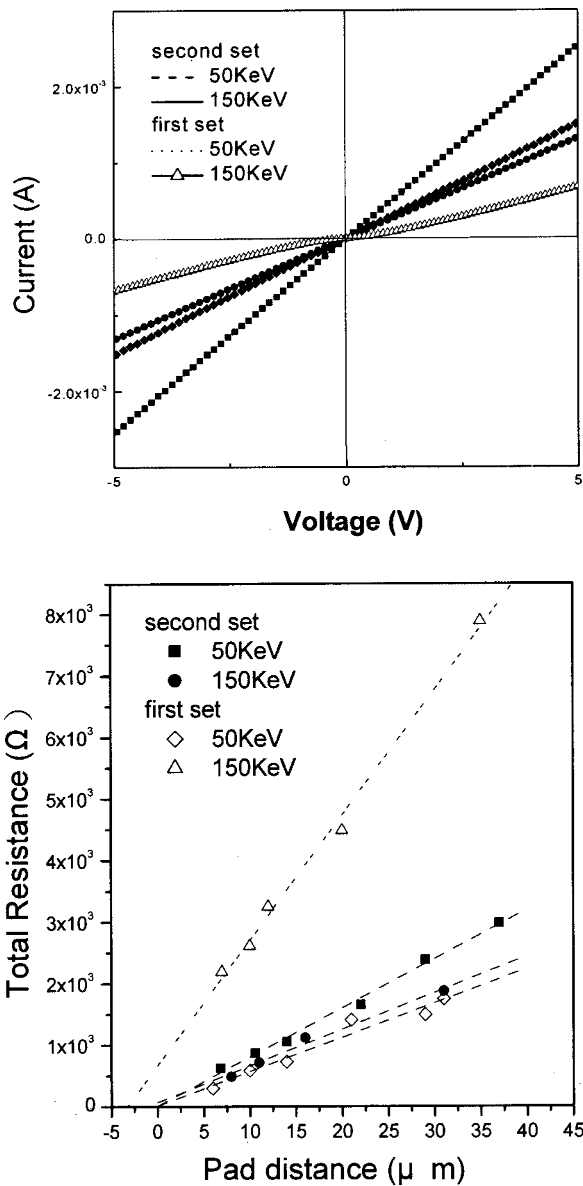

FIG. 8. (a) The $I-V$ curves of Ni/Au and Ni/Pd/Au contacts on high carrier concentration of Be implanted Mg-doped GaN, and (b) CTLM fit results of the Ni/Au and Ni/Pd/Au on high carrier concentration of Be implanted Mg-doped GaN.

$\times 10^{-3}$ $\Omega\,cm^2$ without any further annealing process. For as-grown sample with carrier concentration of 5.5 $\times 10^{16}$ cm^{-3}, no ohmic contact was measured. The results indicated that Be implantation not only enhances the carrier concentration but also facilitates the p-type contact resulting in very low specific resistance ohmic contact, which is most desirable for optoelectronic devices. Table I summarizes the detail results of Hall measurement and specific resistance for both sets of samples.

IV. CONCLUSION

In summary, we investigated the electrical and optical properties of Be implanted Mg-doped GaN and found that the hole concentration was substantial enhanced for the Be implanted samples without post-growth annealing. The hole concentration as high as 8.1×10^{19} cm^{-3} was obtained for samples with RTA at 1100 °C for 60 s. It is also found from the temperature dependent photoluminescence that the activation energy of Mg dopants for the Be implanted samples has an estimated value of about 170 meV, which is nearly 30% lower than the value of typical as-grown samples of about 250 meV. The crystal quality and surface morphology of the Be implanted samples measured by x-ray diffraction and AFM showed no major changes in the crystal quality and surface morphology. The high hole concentration samples also showed very low specific resistance ohmic contact as low as 4.5×10^{-6} $\Omega\,cm^2$ using Ni/Pd/Au metallization. We believe the implantation of Be in p-type GaN samples is an effective and viable method for achieving a high hole concentration and realization of p-type ohmic contact with low specific resistance for p-GaN material.

TABLE I. The hole concentrations and specific resistance of the first and second set samples.

Sample	First set		Second set	
Implant energy (keV)	150	50	150	50
Implant dosage (cm^{-2})	10^{14}	10^{14}	10^{14}	10^{14}
RTA temperature (°C)	1100	1100	1100	1100
Contact metallization	Ni/Au	Ni/Pd/Au	Ni/Pd/Au	Ni/Pd/Au
Carrier concentration (cm^{-3})	2.3×10^{18}	2.3×10^{19}	3.1×10^{18}	8.1×10^{19}
Specific resistance ($\Omega\,cm^2$)	6.9×10^{-3}	9.5×10^{-5}	2.7×10^{-4}	4.5×10^{-6}

ACKNOWLEDGMENTS

This work was supported in part by the National Science Council of Republic of China (ROC) in Taiwan under Contract No. NSC 90-2215-E-009-102 and by the Academic Excellence Program of the ROC Ministry of Education under the Contract No. 88-FA06-AB. The authors would like to thank the Chung-Shan Institute of Science & Technology for providing the MOCVD grown GaN samples, H. W. Huang for the experiment support, and Dr. G. C. Chi of National Central University for the use of the ion implantation facility.

[1] S. Strite and H. Morkoc, J. Vac. Sci. Technol. B **10**, 1237 (1992).
[2] H. Morkoc, S. Strite, G. B. Gao, M. E. Lin, B. Sverdlov, and M. Burns, J. Appl. Phys. **76**, 1363 (1994).
[3] S. J. Pearton, C. B. Vartuli, J. C. Zolper, C. Yuan, and R. A. Stall, Appl. Phys. Lett. **67**, 1435 (1995).
[4] S. Nakamura, T. Mukai, and M. Senoh, Jpn. J. Appl. Phys., Part 2 **30**, L1998 (1991).
[5] F. A. Ponce and D. P. Bour, Nature (London) **386**, 351 (1997).
[6] A. G. Drizhuk, M. V. Zaitev, V. G. Sidorov, and D. V. Sidorov, Tech. Phys. Lett. **22**, 259 (1996).
[7] S. Nakamura and G. Fasol, *The Blue Laser Diode-Gallium-Nitride Based Light Emitters and Laser* (Springer, Berlin, 1997).
[8] B. Goldenberg, J. D. Zook, and R. J. Ulmer, Appl. Phys. Lett. **62**, 381 (1993).
[9] Q. Chen, M. A. Khan, C. J. Sun, and J. W. Yang, Electron. Lett. **31**, 1781 (1995).
[10] E. D. Jungbluth, Laser Focus World **29**, 33 (1993).
[11] D. Walker, A. Saxler, P. Kung, X. Zhang, M. Hamilton, J. Daiz, and M. Razeghi, Appl. Phys. Lett. **72**, 3303 (1998).

[This article is copyrighted as indicated in the article. Reuse of AIP content is subject to the terms at: http://scitation.aip.org/termsconditions. Downloaded to] IP: 140.113.38.11 On: Thu, 01 May 2014 06:11:38

[12] A. V. Andrianov, D. E. Lacklison, J. W. Orton, D. J. Dewsnip, S. E. Hooper, and C. T. Foxon, Semicond. Sci. Technol. **11**, 366 (1996).
[13] F. A. Reboredo and S. T. Pantelides, Phys. Rev. Lett. **82**, 1887 (1999).
[14] C. H. Park and D. J. Chadi, Phys. Rev. B **55**, 12 995 (1997).
[15] C. G. Van de Walle, Phys. Rev. B **56**, R10 020 (1997).
[16] D. J. King, L. Zhang, J. C. Ramer, S. D. Hersee, and L. F. Lester, Mater. Res. Soc. Symp. Proc. **468**, 421 (1997).
[17] T. Mori, T. Kozawa, T. Ohwaki, Y. Taga, S. Nagai, S. Yamasaki, S. Asami, N. Shibata, and M. Koike, Appl. Phys. Lett. **69**, 3537 (1996).
[18] T. Kim, J. Khim, S. Chae, and T. Kim, Mater. Res. Soc. Symp. Proc. **468**, 427 (1997).
[19] F. Bernardini, V. Fiorentini, and A. Bosin, Appl. Phys. Lett. **70**, 2990 (1997).
[20] R. G. Wilson, S. J. Pearton, C. R. Abernathy, and J. M. Zavada, Appl. Phys. Lett. **66**, 2238 (1995).
[21] R. G. Wilson, C. B. Vartuli, S. J. Pearton, C. R. Abernathy, and J. M. Zavada, Solid State Electron. **38**, 1329 (1995).
[22] J. C. Zolper, J. Cryst. Growth **178**, 157 (1997) and references therein.
[23] C. Ronning, M. Dalmer, M. Deicher, M. Restle, H. Hofsass, M. D. Bremser, and R. F. Davis, Mater. Res. Soc. Symp. Proc. **468**, 407 (1997).
[24] J. I. Pankove and J. A. Hutchby, J. Appl. Phys. **47**, 5387 (1976).
[25] J. F. Ziegler, *Handbook of Ion Implantation Technology* (IBM Research, New York, 1992), pp. 2–5.
[26] M. Cardona: *Topics in Applied-Light Scattering in Solids* (Springer, Berlin, 1983), pp. 35–37.
[27] F. Bernardini, V. Fiorentini, and A. Bosin, Appl. Phys. Lett. **70**, 2990 (1997).
[28] J. Hong, J. W. Lee, C. B. Abernathy, J. D. Mackenzie, S. M. Donovan, S. J. Pearton, and J. C. Zoper, J. Vac. Sci. Technol. A **15**, 797 (1997).
[29] F. Shahedipour and B. W. Wessels, Appl. Phys. Lett. **76**, 3011 (2000).
[30] E. Oh, H. Park, and Y. Park, Appl. Phys. Lett. **72**, 70 (1998).
[31] E. Oh, M. Park, S. Kang, H. Cho, B. Kim, M. Yoo, H. Song, and T. Kim, J. Cryst. Growth **189/190**, 537 (1998).
[32] L. Eckey, U. van Gfug, J. Holst, A. Hoffmann, H. Siegle, C. Thomsen, B. Schinneler, K. Heime, M. Henken, O. Schon, and R. Beccard, J. Appl. Phys. **84**, 5828 (1998).
[33] U. Kaufmann, M. Kunzer, M. Maier, H. Obloh, A. Ramakrishnan, B. Santic, and P. Schlotter, Appl. Phys. Lett. **72**, 1326 (1998).
[34] D. J. Dewsnip, A. V. Andrianov, I. Harrison, J. W. Orton, D. E. Lacklison, G. B. Ren, S. E. Hooper, T. S. Cheng, and C. T. Foxon, Semicond. Sci. Technol. **13**, 500 (1998).
[35] M. Leroux, N. Grandjean, B. Beaumont, G. Nataf, F. Semond, J. Massies, and P. Gibart, J. Appl. Phys. **86**, 3721 (1999).
[36] R. Dingle and M. Ilegems, Solid State Commun. **9**, 175 (1971).
[37] D. J. As, T. Simonsmeier, B. Schöttker, T. Frey, D. Schikora, W. Kriegseis, W. Burkhardt, and B. K. Meyer, Appl. Phys. Lett. **73**, 1835 (1998).
[38] C. C. Yu, C. F. Chu, J. Y. Tsai, C. F. Lin, W. H. Lan, C. I. Chiang, and S. C. Wang, Jpn. J. Appl. Phys. **40**, L417 (2001).
[39] C. F. Chu, C. C. Yu, Y. K. Wang, J. T. Tsai, F. I. Lai, and S. C. Wang, Appl. Phys. Lett. **77**, 3423 (2000).

[This article is copyrighted as indicated in the article. Reuse of AIP content is subject to the terms at: http://scitation.aip.org/termsconditions. Downloaded to] IP: 140.113.38.11 On: Thu, 01 May 2014 06:11:38